



Noninvasive optical evaluation of spontaneous low frequency oscillations in cerebral hemodynamics

Ran Cheng^a, Yu Shang^a, Don Hayes Jr.^b, Sibiu P. Saha^c, Guoqiang Yu^{a,*}

^a Center for Biomedical Engineering, College of Engineering, University of Kentucky, USA

^b College of Medicine, The Ohio State University, USA

^c Division of Cardiothoracic Surgery, University of Kentucky, USA

ARTICLE INFO

Article history:

Accepted 24 May 2012

Available online 1 June 2012

ABSTRACT

Spontaneous low frequency oscillations (LFOs) around 0.1 Hz have been observed in mean arterial pressure (MAP) and cerebral blood flow velocity (CBFV). Previous studies have shown that cerebral autoregulation in major arteries can be assessed by quantification of the phase shift between LFOs of MAP and CBFV. However, many cerebral diseases are associated with abnormal microvasculature and tissue dysfunction in brain, and quantification of these abnormalities requires direct measurement of cerebral tissue hemodynamics. This pilot study used a novel hybrid near-infrared diffuse optical instrument to noninvasively and simultaneously detect LFOs of cerebral blood flow (CBF) and cerebral oxygenation (i.e., oxygenated/deoxygenated/total hemoglobin concentration: [HbO₂]/[Hb]/THC) in human prefrontal cortex. Using the hybrid instrument and a finger plethysmograph, the dynamic changes of CBF, [HbO₂], [Hb], THC and MAP were concurrently measured in 15 healthy subjects at rest, during 70° head-up-tilting (HUT) and during enforced breathing at 0.1 Hz. The LFOs were extracted from the measured variables using power spectral analysis, and the phase shifts and coherences of LFOs between MAP and each of the measured hemodynamic variables were calculated from the corresponding transfer functions. Levels of coherence (>0.4) were used to judge the success of LFO measurements. We found that CBF, [HbO₂] and THC were reliable hemodynamic parameters in detecting LFOs and HUT was the most robust and stable protocol for quantifying phase shifts of hemodynamic LFOs. Comparing with other relevant studies, similar success rates for detecting cerebral LFOs have been achieved in our study. The phase shifts of LFOs in CBF were also close to those in CBFV reported by other groups, although the results in cerebral oxygenation measurements during enforced breathing varied across studies. Future study will investigate cerebral LFOs in patients with cerebral impairment and evaluate their cerebral autoregulation capabilities and neurocognitive functions via the quantification of LFO phase shifts.

© 2012 Elsevier Inc. All rights reserved.

Introduction

Spontaneous low frequency oscillations (LFOs) around 0.1 Hz in blood pressure were first described by Mayer (1876). Consequently, LFOs of blood pressure were named “Mayer waves”. These waves are thought to originate from the action of baroreflex in the cardiovascular system (Nilsson and Aalkjaer, 2003). More recently, LFOs have also been observed in cerebral blood flow velocity (CBFV) of the middle cerebral artery detected by transcranial Doppler ultrasound (TCD) (Diehl et al., 1998), in cerebral tissue blood oxygenation measured by near-infrared spectroscopy (NIRS) (Katura et al., 2006), and in the cerebral blood-oxygen-level dependence (BOLD) signal quantified by functional MRI (fMRI) (Biswal et al., 1995). Although the origin of LFOs in cerebral hemodynamics remains unclear, studies

have found that brain exhibits myogenic (Morita et al., 1995), metabolic (Vern et al., 1988) and neurogenic (Auer, 2008) oscillations in the same low frequency range, previously shown to be dominated by sympathetic nervous system activity. It has been known that the myogenic, metabolic, and neurogenic controls are the main mechanisms responsible for maintaining the cerebral blood flow (CBF) constant during blood pressure fluctuations; so-called cerebral autoregulation. Studies of the relationship between LFOs of arterial blood pressure (ABP) and cerebral hemodynamics reveal the CBF control mechanism underlying the blood pressure oscillation, thus holding potential for assessing cerebral autoregulation (Panerai, 2008; Reinhard et al., 2006) and neurocognitive function (Auer, 2008). For example, Reinhard et al. (2006) found declines/increases in phase lead/lag of LFOs between the CBFV/oxygenation and ABP in patients with carotid stenosis. Studies using fMRI demonstrated that cerebral functional connectivity derived from LFO signals of BOLD was different in patients with neurocognitive disease (e.g., Alzheimer disease) compared to healthy controls (Wang et al., 2007).

* Corresponding author at: Center for Biomedical Engineering, University of Kentucky, 600 Rose Street, Lexington, KY 40506, USA. Fax: +1 859 257 1856.

E-mail address: guoqiang.yu@uky.edu (G. Yu).

In studies of LFOs, the finger plethysmography technique is often used for noninvasive and continuous monitoring of ABPs including mean arterial pressure (MAP), systolic blood pressure (SAP), and diastolic blood pressure (DAP) (van Beek et al., 2008). Various noninvasive techniques have attempted to capture LFOs of cerebral hemodynamics including TCD (Diehl et al., 1995, 1998), fMRI (Biswal et al., 1997), NIRS (Obrig et al., 2000; Reinhard et al., 2006), and concurrent fMRI/NIRS (Tong and Frederick, 2010). The CBFV in major arteries measured by TCD may not be consistent with CBF in the microvasculature (Edlow et al., 2010). However, many cerebral diseases, such as stroke and neurocognitive impairment, are associated with abnormal microvasculature and tissue dysfunction in the brain (Bosomtvi et al., 2008; Brown and Thore, 2011). Moreover, TCD cannot be performed on ~9% people who have inadequate acoustic windows (Marinoni et al., 1997). Although fMRI can image cerebral hemodynamics with high spatial resolution, the high cost, low temporal resolution and poor mobility limit its frequent use. NIRS provides a noninvasive, rapid, portable and low-cost alternative to monitor cerebral tissue oxygenation in microvasculature (Boas et al., 2001; Cooper et al., 2011; Fantini et al., 1994; Pogue and Paulsen, 1998; Sassaroli et al., 2011; White et al., 2009). The difference between major tissue chromophores in near-infrared (NIR) absorption spectra enables the measurement of oxygenated ([HbO₂]), deoxygenated ([Hb]), and total hemoglobin concentrations (THC), although NIRS does not directly measure CBF. Cerebral hemodynamic parameters (e.g., CBF and cerebral oxygenation) are usually coupled and interactive. It is thus desirable to simultaneously measure multiple cerebral hemodynamic variables and investigate their relationships.

The measurement of LFOs in the resting state is easy to perform, but usually shows weak oscillations (Diehl et al., 1998, 1999; Haubrich et al., 2004). In order to increase the signal-to-noise ratio (SNR) of LFOs, physiological manipulations have been applied in subjects such as head-up-tilting (HUT) (Diehl et al., 1998, 1999; Haubrich et al., 2004) and enforced breathing at 0.1 Hz (Diehl et al., 1995; Obrig et al., 2000; Reinhard et al., 2006). During HUT, LFOs in cerebral hemodynamics and MAP appear to be elevated due to increased sympathetic nervous activity (Diehl et al., 1998). Enforced breathing superimposes a strong 0.1 Hz oscillation on MAP, thus enhancing LFOs of both MAP and cerebral hemodynamics. However, changing the respiratory rate may create complex chemical and neural reactions that disturb cerebral autoregulation. A comparison of LFOs under different conditions may assist in choosing the experimental protocols to optimize LFOs.

The present study was conducted to determine the feasibility of using a newly-developed hybrid NIR optical instrument (Irwin et al., 2011; Munk et al., 2012; Shang et al., 2009) to simultaneously detect LFOs of CBF and cerebral oxygenation in microvasculature under three different physiological conditions, i.e., at rest, during 70° HUT and during enforced breathing at 0.1 Hz. The hybrid NIR optical instrument we used consists of a custom-designed NIR diffuse correlation spectroscopy (DCS) flowmeter for CBF measurement and a commercial NIRS tissue-oximeter (Imagent, ISS Inc., USA) for cerebral oxygenation measurement. DCS is a relatively new technique which can directly probe blood flow in deep tissues including the cerebral cortex (Cheung et al., 2001; Culver et al., 2005; Dietsche et al., 2007; Durduran et al., 2009, 2010; Edlow et al., 2010; Gagnon et al., 2008; Li et al., 2008; Shang et al., 2011a,b; Zirik et al., 2010). Blood flow variations measured by DCS have been validated in various organs and tissues against other standards, including Doppler ultrasound (Roche-Labarbe et al., 2010), power Doppler ultrasound (Yu et al., 2005), laser Doppler (Durduran, 2004; Shang et al., 2011a), Xenon-CT (Kim et al., 2010), fluorescent microsphere measurement (Zhou et al., 2009), and perfusion MRI (Yu et al., 2007). The hybrid NIR optical instrument offers direct and simultaneous measurements of CBF and cerebral oxygenation in microvasculature within the same region of cerebral cortex, which may bring new and informative insights about LFOs in local brain tissues.

In this study, we have used the hybrid NIR instrument and a finger plethysmograph to measure dynamic changes of CBF, [HbO₂], [Hb], THC and MAP in 15 healthy subjects at rest, during 70° HUT and during enforced breathing at 0.1 Hz. The LFOs were extracted from the measured variables using power spectral analysis (Zhang et al., 1998). The phase shifts and coherences of LFOs between MAP and each of the measured cerebral hemodynamic parameters were calculated from the corresponding transfer functions (Diehl et al., 1998; Obrig et al., 2000; Reinhard et al., 2006). The levels of coherence were then used to select reliable LFOs between the paired signals. Finally, the success rates for capturing LFOs of hemodynamic variables under the three physiological conditions were compared to determine the best hemodynamic parameter(s) and optimal condition(s) in detecting cerebral hemodynamic LFOs.

Method and materials

NIR diffuse optical measurement of cerebral hemodynamics

When using NIRS/DCS to detect tissue blood oxygenation/flow, a pair of source and detector fibers is usually placed on the tissue surface with a distance of a few centimeters. NIR light generated by a laser transmits into tissues through the source fiber and is detected by a photodetector through the detector fiber. The penetration depth of NIR light in biological tissues is approximately half of the source-detector (S-D) separation (Fantini et al., 1994; Irwin et al., 2011). NIRS measures the amplitude reductions and phase shifts of the modulated light (for a frequency-domain system) at multiple wavelengths and multiple S-D separations to extract tissue oxygenation information (Fantini et al., 1994; Irwin et al., 2011). DCS blood flow measurement is accomplished by monitoring speckle fluctuations of photons emitted at the tissue surface (Irwin et al., 2011; Munk et al., 2012; Shang et al., 2009).

DCS for CBF measurement

Details about DCS theory and instrumentation have been described elsewhere (Boas and Yodh, 1997; Cheung et al., 2001; Irwin et al., 2011; J. Li et al., 2008). Briefly, A NIR laser diode with long coherence length (>5 m) transmits light through a source fiber into the tissue. The motions of moving scatterers (primarily red blood cells in the microvasculature) cause light intensity fluctuations on the tissue surface. A single-photon-counting avalanche photodiode (APD) detects temporal intensity fluctuations in a single speckle area on the tissue surface through a single-mode fiber. The output of the APD is sent to an autocorrelator for calculating the normalized light intensity temporal autocorrelation function (g_2). The normalized electric field temporal autocorrelation function (g_1) can be derived from the measured g_2 using the Siegert relation (Rice, 1954). The unnormalized electric field temporal autocorrelation function (G_1) satisfies the correlation diffusion equation in highly scattering media (Boas and Yodh, 1997). The exact form of the correlation diffusion equation depends on the nature and heterogeneity of the particle motion. For the case of diffusive motion, the mean-square displacement, $\langle \Delta r^2(\tau) \rangle$, of the moving scatterers (e.g., red blood cells) in time τ is $\langle \Delta r^2(\tau) \rangle = 6D_B\tau$. Here D_B is an *effective* diffusion coefficient of the moving red blood cells. An α term (0 to 1) is added to account for the fact that not all scatterers in tissue are dynamic and is defined as the ratio of moving scatterers to total scatterers. The combined term, αD_B , is referred to as the blood flow index in biological tissues (Irwin et al., 2011) and is derived by fitting the measured autocorrelation function to the analytical solution of g_2 . The relative CBF (rCBF) denoted as the CBF percentage change relative to its baseline (assigned to be "100%"), is calculated by normalizing the αD_B to its baseline value before physiological changes are initiated.

For this study, we built a two-source and 16-detection-channel DCS flowmeter (see Fig. 1) consisting of two 830 nm laser diodes (100 mW, CrystaLaser Inc., USA), 16 APDs (PerkinElmer Inc., Canada), and a 16-channel autocorrelator (correlator.com, USA). Two identical fiber-optic probes were designed for monitoring CBF responses in two hemispheres. Each probe contained one DCS source fiber (diameter = 200 μm) coupled with one laser diode and one detection fiber bundle connected to 8 APDs. The detection fiber bundle integrated 8 single-mode fibers (core diameter = 5.6 μm) in a small detection area ($\sim 0.16 \text{ mm}^2$) for spatial averaging of 8-channel APD signals to increase the SNR of DCS measurements (Dietsche et al., 2007). We ignored tissue heterogeneity within this small detection area. The use of single-mode fibers for DCS detection limited the measured light intensity, thus restricting the S–D separation. The S–D separation used in this study was set to 2.5 cm, allowing for the detection of CBF in adult prefrontal cortex (Durduran et al., 2004; Edlow et al., 2010; Gagnon et al., 2008; Li et al., 2005; Shang et al., 2011b; Zirak et al., 2010). The 16-channel parallel autocorrelator worked in a burst mode which permitted obtaining 16 autocorrelation function curves in $6.5 \cdot N \text{ ms}$ (Dietsche et al., 2007). Here N is an integer number set by the DCS control panel. The shortest duration (6.5 ms when $N = 1$) to generate the 16 autocorrelation curves was much shorter than that ($\sim 44 \text{ ms}$) using a autocorrelator working in the continuous mode previously (Shang et al., 2009). To get sufficient SNR and adequate sampling rate, this study set N equal to 24. The autocorrelator thus yielded 16 autocorrelation curves every 156 ($24 \cdot 6.5$) ms.

Imagent for cerebral oxygenation measurement

The commercial tissue-oximeter, Imagent (see Fig. 1(b)) (Fantini et al., 1994; Irwin et al., 2011), is a frequency-domain system consisting of 16 laser diodes at 690 and 830 nm (8 diodes for each wavelength) and 2 photomultipliers (PMT). The laser lights are modulated at 110 MHz. Similar to the DCS measurements, two identical fiber-optic probes were used to detect cerebral oxygenation changes in two hemispheres. Each probe had one detector fiber connected to one PMT and 8 source fibers (4 per wavelength) coupled to the laser diodes. The source fibers (diameter = 400 μm) were arranged at distances of 2.0, 2.5, 3.0, 3.5 cm from the detector fiber (diameter = 2.5 mm). The Imagent device measured amplitudes and phases of frequency-modulated light at two wavelengths and four S–D separations (Fantini et al., 1994; Irwin et al., 2011). A simplified solution based on semi-infinite geometry for the photon diffusion equation exposed linear relationships between the phases and logarithmic amplitudes and the S–D separations (Fantini et al., 1994; Irwin et al., 2011). By fitting slopes of these linear relationships, absolute values of tissue absorption coefficient μ_a and reduced scattering coefficient μ_s' can be extracted at each wavelength (Fantini et al., 1994; Irwin et al., 2011). The absolute values of tissue blood oxygenation (i.e., $[\text{HbO}_2]$, $[\text{Hb}]$ and THC) were then calculated from the measured μ_a at the two wavelengths (690 and 830 nm) (Fantini et al., 1994; Irwin et al., 2011).

We found however that the measured time courses of absolute tissue blood oxygenation were too noisy to extract reliable LFOs.

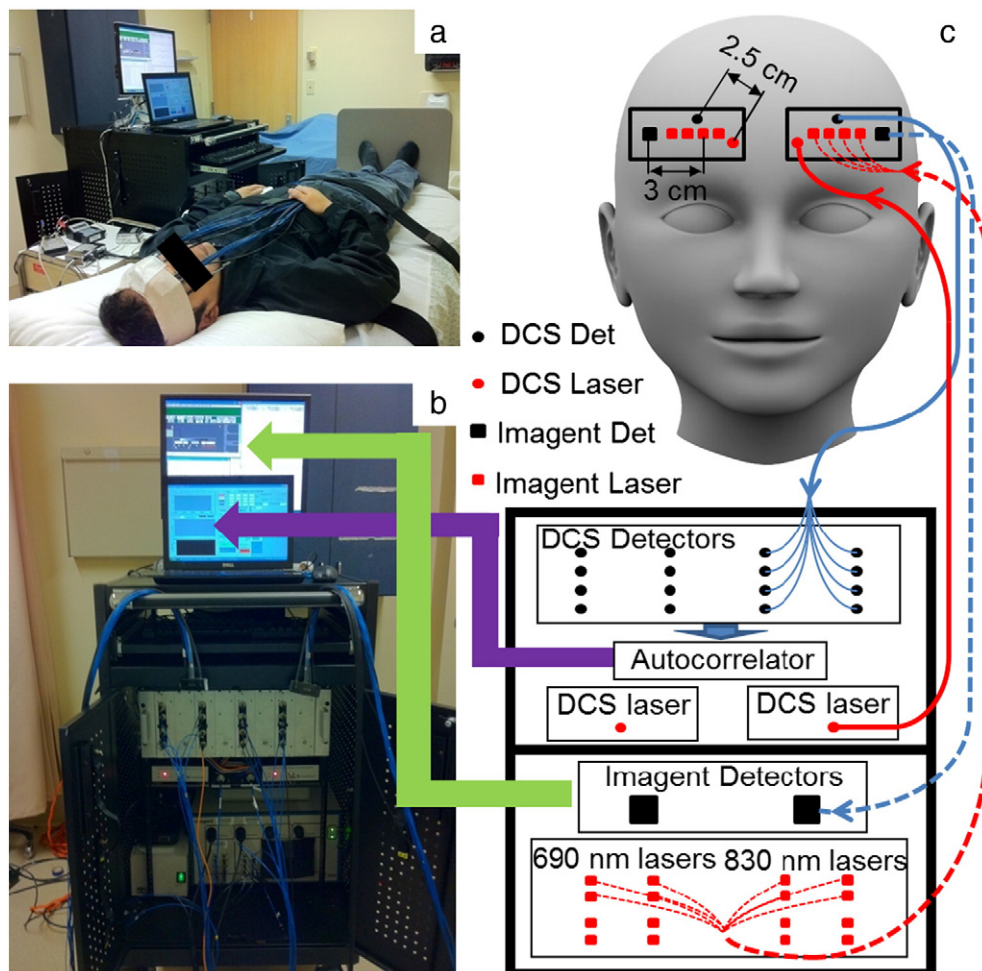


Fig. 1. The NIR hybrid optical instrument for noninvasive measurements of LFOs in cerebral hemodynamics. (a) the experimental setup, (b) a photograph of the hybrid instrument, and (c) the placement of two hybrid fiber-optic probes on the forehead (upper panel) and illustration of the hybrid instrument (lower panel).

This was mainly due to the instability of phase slopes over time. Thus, we ignored the phases from our analysis and used the measured amplitudes at the two wavelengths from a single S–D pair (S–D separation = 3 cm) to calculate the relative changes of cerebral blood oxygenation (i.e., $\Delta[\text{HbO}_2]$ and $\Delta[\text{Hb}]$) (Sassaroli et al., 2011; Zirik et al., 2010). The $\Delta[\text{HbO}_2]$, $\Delta[\text{Hb}]$ and ΔTHC represent the changes of $[\text{HbO}_2]$, $[\text{Hb}]$ and THC relative to their baseline values (assigned to be “0”). According to the modified Beer–Lambert law, $\Delta[\text{HbO}_2]$ and $\Delta[\text{Hb}]$ can be derived from measured light intensity changes relative to their baseline values at the two wavelengths, which depend on extinction coefficients and differential pathlength factors (DPF) at the corresponding wavelengths. The extinction coefficients were determined based on literature (Duncan et al., 1995) and DPF values were calculated using the measured absolute baseline values of μ_a and μ_s' (Fantini et al., 1999; Irwin et al., 2011), and were assumed constant over time. The ΔTHC were then calculated by summing the $\Delta[\text{HbO}_2]$ and $\Delta[\text{Hb}]$.

Hybrid instrument for CBF and cerebral oxygenation measurement

In order to simultaneously measure CBF and cerebral oxygenation, the 16-channel DCS was combined with the Imagent to form a hybrid NIR optical instrument (see Fig. 1(b)). Two hybrid fiber-optic probes connected to the hybrid NIR instrument were placed on the left and right sides of the forehead for bilateral cerebral measurements (see Fig. 1(c)). In each probe, the lasers for DCS and Imagent measurements were turned on sequentially to avoid the light interference between flow and oxygenation measurements. However, since the light emitted from one probe did not affect the detectors in another probe, bilateral measurements were conducted concurrently. The sampling time for one frame of cerebral hemodynamic data was ~500 ms (equivalent to a sampling rate $f_s = 2$ Hz) which included ~250 ms for Imagent measurement, ~150 ms for DCS measurement, and ~100 ms for switching between the two measurements. The communication between the two devices (through digital I/O lines) and data acquisition were controlled by custom-designed software installed on the two control panels (computers) for DCS and Imagent, respectively (Irwin et al., 2011; Munk et al., 2012; Shang et al., 2009).

Experimental protocols

Fifteen young healthy adults (10 males and 5 females) participated in this study with signed consent forms approved by the University of Kentucky Institutional Review Board (IRB). The average age of the subjects was 27 ± 5 years.

Cerebral hemodynamic parameters and MAP were simultaneously measured by the hybrid NIR optical instrument and a finger plethysmograph under three conditions: at rest, during HUT and during enforced breathing at 0.1 Hz. Each subject was asked to lie supine on a tilting table (Hausmann Inc., USA), and two Velcro straps were placed over the chest and thighs to immobilize the body. The left forearm was placed at heart level on a padded cushion. Beat-to-beat MAP (mm Hg) was monitored continuously via a noninvasive finger plethysmograph (Portapres, FMS Inc., Netherlands). The plethysmograph sensor was fixed on the middle finger of left hand. Two fiber-optic probes were taped respectively on the left and right sides of the forehead at a position about 2 cm from the midline and 1 cm above the eyebrows. A self-adhesive elastic band was then stretched around the forehead to fix both probes tightly and minimize the influence of room light on optical measurements. Optical data were continuously recorded throughout the experimental protocols which included 10 min baseline at rest, 10 min HUT up to 70°, 10 min break after HUT back to 0°, and 10 min enforced breathing at 0.1 Hz. During HUT test, an adjustable medical sling was used to hold the left forearm and keep the plethysmograph sensor at the heart level. Prior to the test, each subject

was trained to breathe regularly at 0.1 Hz following audio cues made by Microsoft PowerPoint. Room light was turned off during experiments to minimize the influence of ambient light.

Calculation of LFO intensity

Following methods used in previous studies (Diehl et al., 1998; Obrig et al., 2000; Reinhard et al., 2006), LFO intensities of MAP and cerebral hemodynamic parameters (i.e., rCBF, $\Delta[\text{HbO}_2]$, $\Delta[\text{Hb}]$, and ΔTHC) under the three physiological conditions (i.e., at rest, during HUT, and during enforced breathing at 0.1 Hz) were extracted from their power spectral densities (PSDs) calculated using Welch's method (see Fig. 2) (Zhang et al., 1998). Briefly, the 10 min time-course dataset (~1200 data points at a sampling rate $f_s = 2$ Hz) for each parameter under a specific physiological condition was first detrended to remove baseline shifts. Detrended data were then divided into 8 segments (Reinhard et al., 2006) with 50% overlap in two adjacent segments (Zhang et al., 1998), resulting in a length of ~267 (1200*2/9) data points for each segment. After applying a Hanning window to reduce the effect of spectral leakage, the frequency-domain spectrum of each segment was determined by fast Fourier transform: $\text{FFT}(x_{\text{seg}})$. Here x_{seg} represented one segment of time-course data. Averaging the 8 spectra yielded one smooth spectrum $F_x(f)$ with a frequency resolution of ~0.0075 Hz ($f_s/267$), where f was the frequency. The LFO intensity was defined as $\text{PSD}_{xx}(f) = F_x^*(f) F_x(f) / f_s$, where $F_x^*(f)$ was the complex conjugate of $F_x(f)$ and f was in the low frequency range of 0.05 to 0.15 Hz.

Quantification of the phase relationships between LFOs in MAP and each of the cerebral hemodynamic parameters

Cerebral autoregulation has been assumed to be a linear system with MAP as input and parameters of cerebral hemodynamics as outputs (Diehl et al., 1998; Obrig et al., 2000; Reinhard et al., 2006). A property of linear systems (e.g., phase shifts between the inputs and outputs) can be quantified by transfer function analysis to reveal the characteristics of cerebral autoregulation. In order to perform transfer function analysis, cross spectral densities (CSDs) between MAP and each of the cerebral hemodynamic parameters were calculated similar to the calculation for PSD: $\text{CSD}_{xy}(f) = F_x^*(f) F_y(f) / f_s$ (see Fig. 2), where x and y represented MAP and one of the cerebral hemodynamic parameters, respectively. The transfer function was then calculated: $H(f) = \text{CSD}_{xy}(f) / \text{PSD}_{xx}(f)$, where the $\text{PSD}_{xx}(f)$ represented the PSD of MAP. The phase shift and coherence between the paired signals were derived from the equations: $\Phi(f) = \arctan[\text{Im}(H(f)) / \text{Re}(H(f))]$ and $\text{Coh}(f) = |\text{CSD}_{xy}(f)|^2 / [\text{PSD}_{xx}(f) \text{PSD}_{yy}(f)]$, where $\text{Im}(f)$ and $\text{Re}(f)$ were the imaginary and real parts of $H(f)$, respectively.

A high level of coherence means a constant and reliable phase relationship between paired variables. The $\text{Coh}(f)$ was thus used to judge the success of LFO measurements and to select reliable phase shifts. According to previous studies (Hu et al., 1999; Reinhard et al., 2003), LFO measurements were judged to be successful if the largest $\text{Coh}(f_0)$ found in the low frequency range ($0.05 < f_0 < 0.15$ Hz) was higher than 0.4. The f_0 and $\Phi(f_0)$ were thus recorded as reliable LFO frequency and phase shift respectively. The positive $\Phi(f_0)$ indicated that the corresponding LFO of a hemodynamic parameter preceded the LFO of MAP in time. LFO leading time (T_{leading}) was calculated from the equation: $T_{\text{leading}} = \Phi(f_0) / 360^\circ / f_0$. The success rates of capturing reliable LFOs and phase shifts for all hemodynamic parameters under the three conditions in two hemispheres were then compared to determine the best parameter(s)/protocol(s) for future studies in different patient populations. A flowchart is plotted in Fig. 2 for better understanding the procedures for data analysis described above.

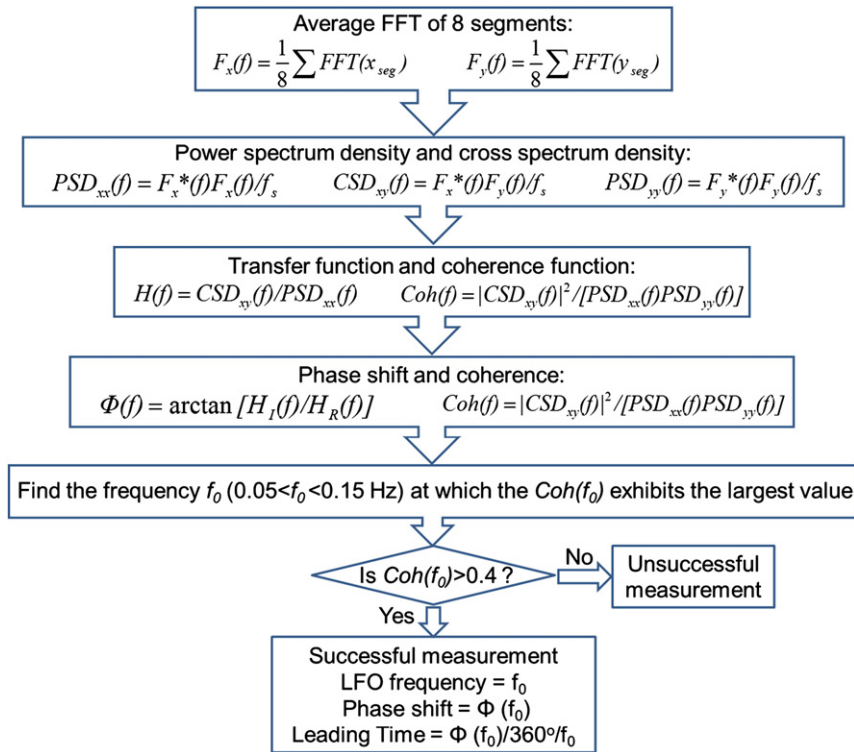


Fig. 2. The data analysis procedures to identify successful LFO measurements and extract phase shifts and leading times in cerebral hemodynamic parameters.

Results

Individual time-course results during physiological manipulations

Fig. 3 shows the typical time-course data of MAP and cerebral hemodynamics throughout the entire protocol measured from one subject's left and right hemispheres. The average levels of MAP at all physiological conditions were similar (~80 mm Hg) over the entire experiment (see Fig. 3(a)). Although slight differences existed in cerebral hemodynamics between the left and right hemispheres (especially during HUT) due to cerebral heterogeneous responses, trends of

bilateral responses were same. The $\Delta[\text{HbO}_2]$ and $\Delta[\text{Hb}]$ showed inverse responses and larger changes were found in $\Delta[\text{HbO}_2]$. The ΔTHC , a combination of $\Delta[\text{HbO}_2]$ and $\Delta[\text{Hb}]$, thus followed the larger change of $\Delta[\text{HbO}_2]$. At rest, cerebral hemodynamic variables were relatively stable as there were no physiological changes. As expected, rCBF decreased during HUT due to the decrease of cardiac output as well as the increase of cerebral vasculature resistance induced by orthostatic stress (Levine et al., 1994). The reduced rCBF led to the decrease in oxygen delivery. As a result, $\Delta[\text{HbO}_2]$ decreased and $\Delta[\text{Hb}]$ increased. During enforced breathing, MAP and cerebral hemodynamics of this subject showed slight variations. In total, eight out of 15 subjects had

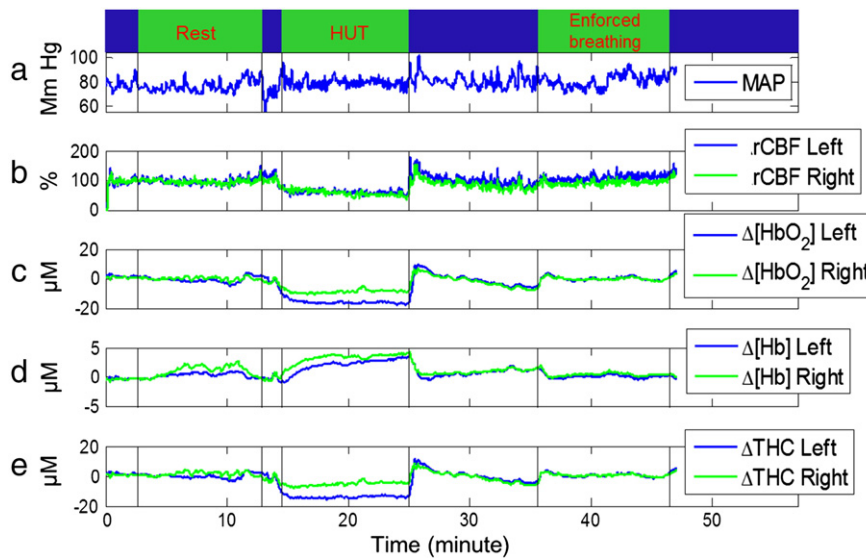


Fig. 3. Typical time-course responses of MAP and cerebral hemodynamics in one subject through the entire experiment. (a) MAP measured by the finger plethysmograph, (b) relative cerebral blood flow (rCBF) and (c) to (e): cerebral oxygenation changes measured in the left and right hemispheres, i.e., (c) $\Delta[\text{HbO}_2]$, (d) $\Delta[\text{Hb}]$, (e) ΔTHC . The vertical lines indicate the beginning and ending of different physiological conditions.

a trend similar to this subject. However, the other seven subjects exhibited slight decreases in rCBF and $\Delta[\text{HbO}_2]$ during enforced breathing (data not shown). The relatively deep and slow controlled breathing at 0.1 Hz may induce hypocapnia (Reinhard et al., 2003), leading to vasoconstriction. As a result, rCBF and $\Delta[\text{HbO}_2]$ decreased in those subjects.

Individual frequency-domain results during physiological manipulations

Fig. 4 shows typical PSDs of all measured parameters at the three physiological conditions, which were calculated from the time-course hemodynamic data obtained from the same subject shown in Fig. 3. Only data obtained from the left hemisphere are presented since similar results were found in the right hemisphere. At rest, small PSD peaks in the low frequency range appeared in MAP (see Fig. 4(a1)) and rCBF (see Fig. 4(b1)). During HUT, PSD signals of all physiological parameters in the low frequency range were substantially enhanced, resulting in obvious peaks around 0.08 Hz (see Figs. 4(a2), (b2), (c2), (d2), and (e2)). Similar to HUT, the enforced breathing at 0.1 Hz generated PSD peaks of all parameters around 0.1 Hz (see Figs. 4(a3), (b3), (c3), (d3), and (e3)). The magnitude of PSD(f) in the low frequency range (0.05 to 0.15 Hz) represents the intensity of LFO. Both HUT and enforced breathing significantly increased the SNR of LFOs in MAP and cerebral hemodynamic variables. Among the physiological parameters, $\Delta[\text{Hb}]$ had the least SNR in detecting LFOs (see Figs. 4(d1), (d2), (d3)).

Fig. 5 demonstrates the relationship (phase shift and coherence) between the LFOs of each paired signals obtained from the left hemisphere of the same subject (see Figs. 3 and 4). Similar results were found in the right hemisphere (data not shown). At rest, coherences were low for all paired variables; only a few points had $\text{Coh}(f)$ higher than 0.4 (see Figs. 5(a1), (b1), (c1), (d1)). During HUT and enforced breathing at 0.1 Hz, coherences were mostly higher than 0.4 in the low frequency range of 0.05 to 0.1 Hz (see Figs. 5(a2), (b2), (d2)) or 0.09 to 0.11 Hz (see Figs. 5(a3), (b3), (c3), (d3)), except the pair of $\Delta[\text{Hb}]$ and MAP (see Fig. 5(c2)).

Average frequency-domain results over subjects

Fifteen healthy subjects were measured in this study. Fig. 6 shows the average PSDs of MAP and cerebral hemodynamic parameters in

the left hemispheres over 15 subjects under the three physiological conditions. Data are presented as mean \pm standard error. Similar results were found in the right hemispheres (data not shown). The trends of average PSDs were similar to those of individual PSDs shown in Fig. 4. The average LFO amplitudes in $\Delta[\text{Hb}]$ under all physiological conditions ($\leq 0.23 \mu\text{M}^2/\text{Hz}$) were smaller than those in $\Delta[\text{HbO}_2]$ ($\geq 0.69 \mu\text{M}^2/\text{Hz}$) and ΔTHC ($\geq 0.32 \mu\text{M}^2/\text{Hz}$). Both HUT and enforced breathing generated large increases in LFO amplitudes, compared to resting state.

The acceptance of reliable LFOs and phase shifts was judged by coherence levels larger than 0.4 (see Method and materials section). Table 1 summarizes LFO frequencies, phase shifts, leading times, and success rates for detecting reliable LFOs. Data are presented as mean \pm standard deviation unless otherwise noted. Since LFO leading times were calculated from the phase shifts, they provided equivalent information about the relationship between MAP and cerebral hemodynamic parameters. For simplicity, we only discuss phase shifts in this paper. Due to the large signal variations ($92.6^\circ \leq \text{std}(\Phi) \leq 122.4^\circ$) and low success rates (47 to 87%), $\Delta[\text{Hb}]$ results (see Table 1) are excluded in following reports.

At rest, the success rates for obtaining reliable LFOs were relatively low (67 to 87%). In addition, the LFO frequencies exhibited a relatively large range (0.078 to 0.086 Hz). The standard deviations of phase shifts were relative large ($32.8^\circ \leq \text{std}(\Phi) \leq 49.9^\circ$). Also, relatively large differences between phase shifts in left and right hemispheres were observed in cerebral hemodynamic parameters ($7.5^\circ \leq |\Phi_{\text{left}} - \Phi_{\text{right}}| \leq 19.6^\circ$).

During HUT, all hemodynamic parameters (except $\Delta[\text{Hb}]$) from both hemispheres showed a 100% success rate in capturing LFOs. LFO frequencies were at ~ 0.076 Hz. The standard deviations of phase shifts were much smaller ($11.8^\circ \leq \text{std}(\Phi) \leq 22.5^\circ$) than those at rest (see Table 1). Minor differences in phase shifts were found between left and right hemispheres ($0.4^\circ \leq |\Phi_{\text{left}} - \Phi_{\text{right}}| \leq 5.6^\circ$).

Similar to HUT, rCBF, $\Delta[\text{HbO}_2]$ and ΔTHC exhibited high success rates (93 to 100%) during enforced breathing at 0.1 Hz. As expected, LFO frequencies were at ~ 0.1 Hz. However, the standard deviations of phase shifts were much larger ($32.7^\circ \leq \text{std}(\Phi) \leq 45.4^\circ$ for $\Delta[\text{HbO}_2]$ and $80.4^\circ \leq \text{std}(\Phi) \leq 88.9^\circ$ for rCBF) than those during HUT (see Table 1). Differences in phase shifts between left and right hemispheres ($8.6^\circ \leq |\Phi_{\text{left}} - \Phi_{\text{right}}| \leq 10.8^\circ$) were also larger than those observed during HUT.

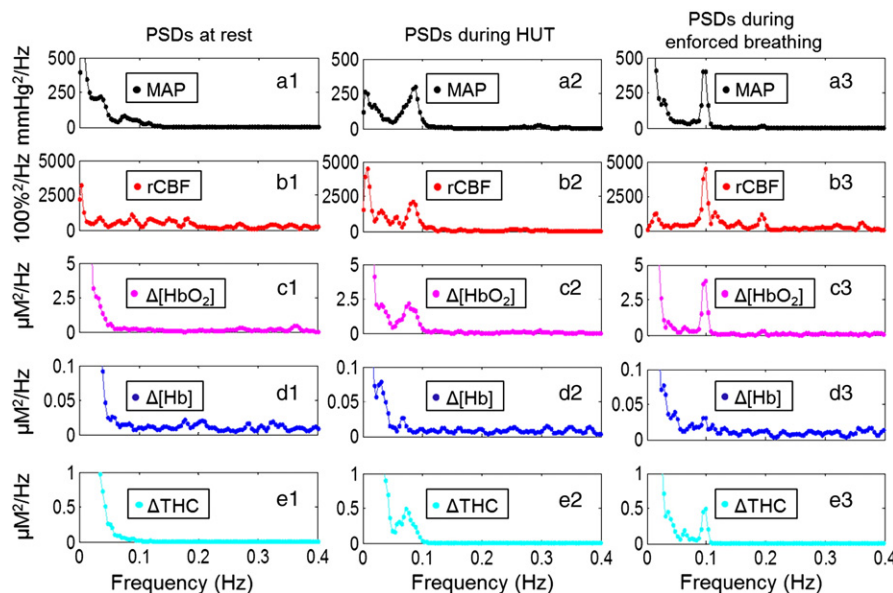


Fig. 4. The PSDs of MAP and cerebral hemodynamics under the three physiological conditions in the subject's left hemisphere. (a1), (b1), (c1), (d1) and (e1): PSDs at rest; (a2), (b2), (c2), (d2) and (e2): PSDs during HUT; (a3), (b3), (c3), (d3) and (e3): PSDs during enforced breathing.

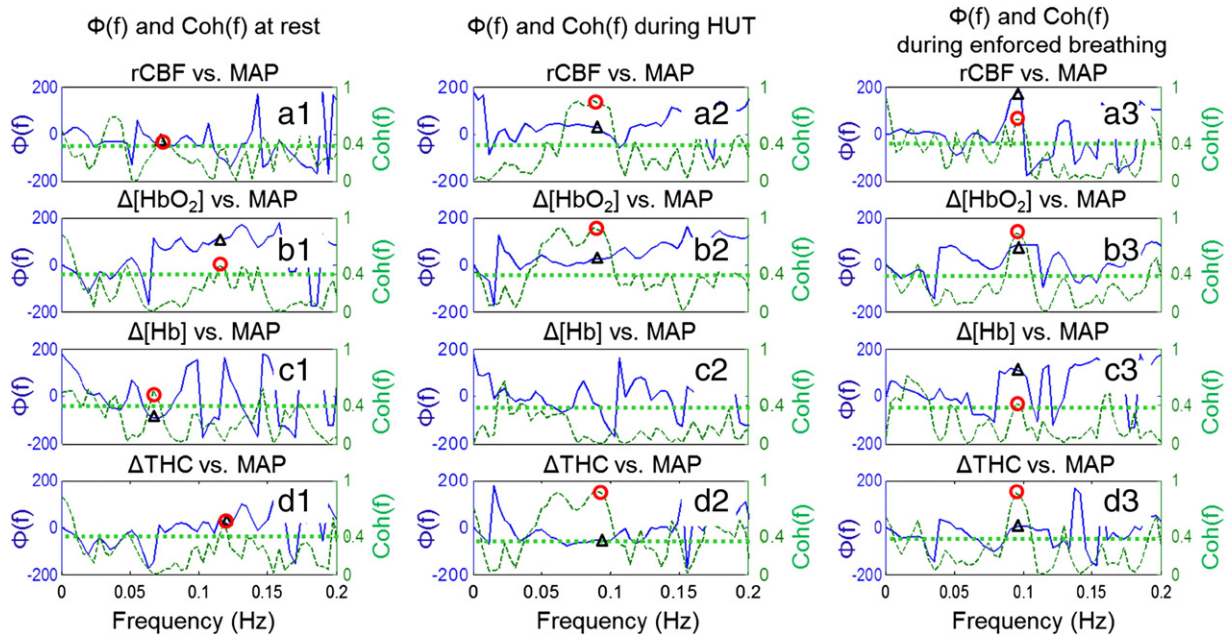


Fig. 5. The phase ($\Phi(f)$) and coherence ($Coh(f)$) spectra of paired signals between MAP and each of the cerebral hemodynamics under the three physiological conditions in the subject's left hemisphere. (a1), (b1), (c1) and (d1): spectra at rest; (a2), (b2), (c2) and (d2): spectra during HUT; (a3), (b3), (c3) and (d3): spectra during enforced breathing. The solid lines represent the $\Phi(f)$ and the dashed lines represent the $Coh(f)$. The horizontal dashed lines indicate the coherence threshold $Coh = 0.4$. The triangles indicate the most reliable phase shifts within the low frequency range. The circles indicate the largest coherences within the low frequency range.

Discussion

NIR diffuse optical technologies enable detection of LFOs in cerebral hemodynamics

Previous studies have shown that quantification of the phase shift between LFOs in ABP and CBFV (measured by TCD) of major arteries can be used for evaluation of cerebral autoregulation in large vessels (Panerai, 2008; Reinhard et al., 2006). However, the CBFV in large arteries does not always reflect the CBF in brain microvasculature (Edlow et al., 2010). Although NIRS has been used to study LFOs in brain microvasculature (Obrig et al., 2000; Reinhard et al., 2006), it cannot directly measure CBF. Moreover, CBF and cerebral tissue

oxygenation are usually coupled and interactive. Thus, direct and simultaneous measurements of multiple cerebral hemodynamic parameters in microvasculature are appealing. However, only a few studies have attempted to detect CBFV and cerebral oxygenation simultaneously (Reinhard et al., 2006; van Beek et al., 2012). In the present study, we demonstrate, *for the first time*, that DCS can detect LFOs of CBF and that the hybrid optical instrument combining DCS and NIRS can simultaneously capture multiple LFOs of cerebral hemodynamic variables (i.e. CBF, $[HbO_2]$, $[Hb]$ and THC). Using two hybrid fiberoptic probes, multiple hemodynamic variables acquired simultaneously from both cerebral hemispheres were successfully measured and used to extract cerebral LFOs. The success rates for capturing LFOs of hemodynamic variables under the three physiological conditions

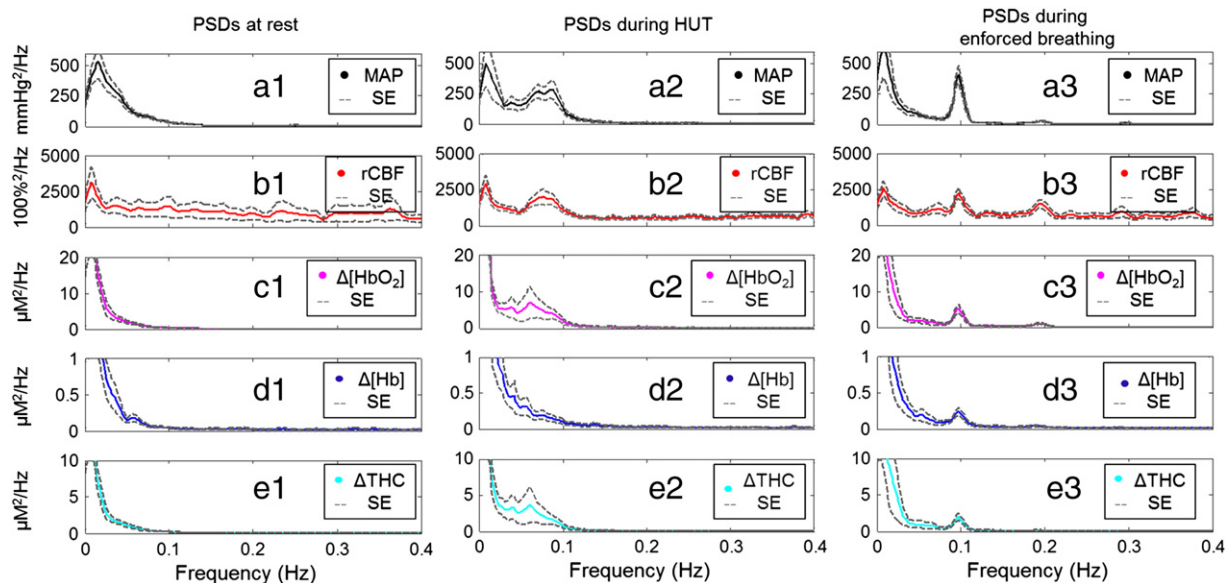


Fig. 6. The average PSDs of MAP and cerebral hemodynamic parameters over subjects ($n = 15$) under the three physiological conditions in the left hemispheres. The solid curves indicate the mean value of PSDs while the dashed curves surrounding the solid curve represent the range of data variations (standard errors).

Table 1
Average LFO frequencies, phase shifts, leading times, and success rates of cerebral hemodynamic LFO measurements.

Number of subjects (n = 15)	Significant level of Coh (Coh > 0.4)	Average LFO frequencies (Hz)			
		rCBF	$\Delta[\text{HbO}_2]$	$\Delta[\text{Hb}]$	ΔTHC
At rest		Average phase shifts (deg)			
Left side		Average leading times (s)			
Right side		(Number of successful measurements; success rates)			
At rest		0.078 ± 0.011	0.079 ± 0.012	0.080 ± 0.010	0.078 ± 0.012
Left side		49.3 ± 46.2	48.6 ± 48.2	4.7 ± 122.4	23.6 ± 44.8
Right side		1.77 ± 1.72	1.54 ± 1.65	0.08 ± 3.84	0.76 ± 1.48
		(13; 87%)	(10; 67%)	(7; 47%)	(11; 73%)
HUT		0.086 ± 0.014	0.084 ± 0.010	0.080 ± 0.008	0.083 ± 0.010
Left side		29.7 ± 49.9	41.1 ± 32.8	-31.1 ± 92.6	7.0 ± 35.9
Right side		0.95 ± 1.61	1.27 ± 1.17	-0.93 ± 3.11	0.26 ± 1.22
		(12; 80%)	(11; 73%)	(9; 60%)	(11; 73%)
Enforced breathing at 0.1 Hz		0.076 ± 0.010	0.076 ± 0.010	0.074 ± 0.009	0.076 ± 0.009
Left side		45.7 ± 19.1	29.5 ± 11.8	-38.1 ± 117.1	-11.3 ± 16.6
Right side		1.65 ± 0.65	1.16 ± 0.59	-1.18 ± 4.09	-0.37 ± 0.53
		(15; 100%)	(15; 100%)	(11; 73%)	(15; 100%)
At rest		0.076 ± 0.010	0.076 ± 0.010	0.076 ± 0.011	0.076 ± 0.009
Left side		45.3 ± 16.7	24.4 ± 12.7	-45.6 ± 99.6	-16.9 ± 22.5
Right side		1.66 ± 0.63	0.96 ± 0.59	-1.48 ± 4.06	-0.54 ± 0.69
		(15; 100%)	(15; 100%)	(13; 87%)	(15; 100%)
Enforced breathing at 0.1 Hz		0.098 ± 0.003	0.097 ± 0.002	0.098 ± 0.007	0.097 ± 0.002
Left side		68.0 ± 88.9	68.9 ± 45.4	-16.2 ± 111.3	20.1 ± 41.4
Right side		2.14 ± 2.40	1.42 ± 0.82	-0.03 ± 2.91	0.57 ± 1.24
		(14; 93%)	(14; 93%)	(13; 87%)	(15; 100%)
At rest		0.097 ± 0.002	0.098 ± 0.003	0.097 ± 0.002	0.097 ± 0.002
Left side		77.7 ± 80.4	60.3 ± 32.7	-22.9 ± 99.7	9.3 ± 41.6
Right side		2.60 ± 2.11	1.66 ± 0.93	-0.97 ± 3.04	0.47 ± 1.24
		(14; 93%)	(15; 100%)	(13; 87%)	(15; 100%)

(i.e., at rest, during HUT and during enforced breathing) were compared to determine the best hemodynamic parameters and physiological conditions for future patient population studies. Finally, the quantitative results obtained from the present experiments were compared to previous studies.

Comparison of LFOs among different hemodynamic variables under different physiological conditions

Among the hemodynamic parameters measured under the three physiological conditions, the LFOs of rCBF, $\Delta[\text{HbO}_2]$ and ΔTHC were detected at reasonable success rates ($\geq 67\%$) and with relatively stable phase shifts ($\text{std}(\Phi) \leq 88.9^\circ$). The LFOs of $\Delta[\text{Hb}]$ were much weaker compared to other variables, which is consistent with previous observations (Obrig et al., 2000; Reinhard et al., 2006). As a result, the phase shifts of $\Delta[\text{Hb}]$ had large variations. Thus it is difficult to determine the relative phase relationship (lead or lag) between $\Delta[\text{Hb}]$ and each of the other parameters (i.e., MAP, rCBF, $\Delta[\text{HbO}_2]$, and ΔTHC). The weak LFOs of $\Delta[\text{Hb}]$ are likely due to the fact that cerebral blood has a high oxygen saturation varying from almost 100% in arterial blood to ~60% in venous blood, resulting in a low ratio of $\Delta[\text{Hb}]$ to $\Delta[\text{HbO}_2]$ (Tong and Frederick, 2010). It is also possible that the cerebral vein (containing more [Hb]) is less reactive to blood pressure variations than is the artery (containing more $[\text{HbO}_2]$) (McCulloch et al., 1982). As a result, $\Delta[\text{Hb}]$ demonstrated the least magnitude and SNR of LFOs, and was thus excluded from the following discussions.

LFOs at rest were weak, leading to low SNRs (Reinhard et al., 2003). As a result, low success rates and large variations (standard derivations) in LFO frequencies, phase shifts, and phase differences between two hemispheres were observed at rest. Both HUT and enforced breathing significantly enhanced LFOs although the mechanisms are different. The enforced breathing enhanced LFOs at 0.1 Hz through respiration-induced MAP oscillation (Reinhard et al., 2003). However, large inter-subject variations in phase shifts of cerebral hemodynamics

were found, which might result from the heterogeneous responses to enforced breathing among subjects. The relatively deep and slow breathing pattern used may induce hypocapnia, leading to increased variations in cerebral hemodynamics (Reinhard et al., 2003). By contrast, the HUT enhanced LFOs most likely through elevated sympathetic activity (Diehl et al., 1998; Levine et al., 1994); it has been found that a single sympathetic burst can initiate a cycle of increasing and decreasing arterial pressure at ~0.1 Hz through the baroreflex feedback loop (Julien, 2006). During HUT, the sympathetic activity bursts in series every ~10 s (Furlan et al., 2000), which can significantly increase LFOs of MAP through baroreflex resonance. Moreover, the HUT protocol is more objective and easier to control compared to the enforced breathing protocol.

Overall, among cerebral hemodynamic variables, $\Delta[\text{Hb}]$ had the lowest success rates for detecting LFOs and the largest inter-subject variations under all three physiological conditions. Among the three physiological conditions, signals obtained during HUT were most robust (highest success rates) and stable (smallest standard deviations).

Comparison of LFO measurements with other studies

Research groups have studied LFOs in cerebral hemodynamics at rest (Diehl et al., 1998, 1999; Haubrich et al., 2004), during HUT (Diehl et al., 1998, 1999; Haubrich et al., 2004) and during enforced breathing at 0.1 Hz (Diehl et al., 1995; Obrig et al., 2000; Reinhard et al., 2006) using transfer function analysis. However, there have been no reports of quantifying cerebral LFOs under all three physiological conditions in a single study. Therefore, we compare our results to those with comparable data in corresponding studies.

At rest, phase shifts and success rates of LFOs in CBF measured by DCS ($29.7^\circ \leq \Phi \leq 49.3^\circ$, $80\% \leq \text{success rate} \leq 87\%$, $n = 15$) are in reasonable agreement with those of CBFV measured by TCD ($44.9^\circ \leq \Phi \leq 56.3^\circ$, $92\% \leq \text{success rate} \leq 100\%$, $20 \leq n \leq 50$) (Diehl et al., 1998, 1999; Haubrich et al., 2004).

During HUT, our results of LFOs in CBF ($45.3^\circ \leq \Phi \leq 45.7^\circ$, success rate = 100%, $n = 15$) are consistent with those in CBFV ($40.6^\circ \leq \Phi \leq 50.2^\circ$, success rate = 100%, $20 \leq n \leq 47$) (Diehl et al., 1998, 1999; Haubrich et al., 2004).

It is not surprising that the enforced breathing at 0.1 Hz makes the LFO frequencies obtained in the present study highly consistent with other studies (Diehl et al., 1995; Obrig et al., 2000; Reinhard et al., 2006). During enforced breathing, our success rates for detecting reliable LFOs of cerebral hemodynamics ($\geq 93\%$ for rCBF and $\Delta[\text{HbO}_2]$, 100% for ΔTHC , $n = 15$) are close to those (100% for CBFV and $\Delta[\text{HbO}_2]$, 97% for ΔTHC , $n = 38$) reported by Reinhard et al. (2006). The phase shifts in CBF ($68.0^\circ \leq \text{std}(\Phi) \leq 77.7^\circ$, $n = 15$) are also similar to those in CBFV ($64.8^\circ \leq \Phi \leq 70.5^\circ$, $38 \leq n \leq 50$) (Diehl et al., 1995; Reinhard et al., 2006). However, inter-subject variations of the phase shifts in CBF ($80.4^\circ \leq \text{std}(\Phi) \leq 88.9^\circ$, $n = 15$) observed in the present study are much larger than those in CBFV ($26.1^\circ \leq \text{std}(\Phi) \leq 29.8^\circ$, $38 \leq n \leq 50$) (Diehl et al., 1995; Reinhard et al., 2006). These large variations might be due to the fact that the CBF of the microvasculature is more sensitive to the hypocapnia induced by the enforced respiration than the CBFV in large cerebral vessels (Segal, 2005). Furthermore, the phase shifts of $\Delta[\text{HbO}_2]$ ($68.9 \pm 45.4^\circ$ for the left hemisphere and $60.3 \pm 32.7^\circ$ for the right hemisphere, $n = 15$) are quite different from the results measured by Reinhard et al. ($\Phi = -23.5 \pm 23.9^\circ$, $n = 38$) and Obrig et al. ($\Phi = -0^\circ$, $n = 3$) (Obrig et al., 2000; Reinhard et al., 2006). Phase shifts of LFOs in ΔTHC are also found different between our measurements ($20.1 \pm 41.4^\circ$ for the left hemisphere and $9.3 \pm 41.6^\circ$ for the right hemisphere, $n = 15$) and those ($\Phi = -22.6 \pm 30.5^\circ$, $n = 38$) reported by Reinhard et al. (2006). The reasons for these differences are unclear although several factors are likely to be involved, including age and number of subject differences among studies, tissue heterogeneity responses (e.g., different penetration depths using different S–D separations of 3 to 5 cm for oxygenation measurements),

instrumentation differences (e.g., frequency-domain versus continuous-wave), subject training differences for controlled breathing, and vascular reactivity differences in response to CO₂ oscillations during enforced breathing.

In the present study, all cerebral hemodynamic LFO phases are referenced to MAP (as zero time reference) measured by finger plethysmograph, allowing us to compare our results with previous works (Diehl et al., 1998, 1999; Haubrich et al., 2004; Obrig et al., 2000; Reinhard et al., 2006). Unlike MAP signals detected from the finger, both rCBF and cerebral oxygenation are measured from a similar region of prefrontal cortex. Using rCBF (instead of MAP) as zero time reference may improve the coherence among cerebral hemodynamic oscillation signals, thus enabling to obtain more reliable results in evaluating phase shifts of cerebral hemodynamic LFOs.

Study limitations

The uses of 2.5 cm S–D separation for DCS detection of CBF (Edlow et al., 2010; Shang et al., 2011b; Zirak et al., 2010) and 3 cm S–D separation for NIRS monitoring of cerebral oxygenation (Obrig et al., 2000; Sassaroli et al., 2011) have been demonstrated and validated previously in various human studies. Also, Monte Carlo simulations of NIR light paths in the human brain have shown that the 2.5 cm and 3 cm S–D separations used in our study are sufficient to detect tissue hemodynamics in cerebral prefrontal cortex (T. Li et al., 2011). In addition, the sensitive regions and penetration depths of NIR measurements with S–D separations of 2.5 cm and 3 cm are similar. However, it should be noticed that optical fibers in our hybrid probe were arranged in a particular pattern (see Fig. 1(c)) for reducing the interference between DCS and NIRS measurements (Shang et al., 2009). As a result, the center of our DCS fiber pair was not aligned precisely with the center of NIRS fiber pairs in the plane of forehead, which may cause certain discrepancy between DCS and NIRS measurements due to tissue heterogeneity responses from different regions.

Although S–D separations of 2.5 and 3 cm have been broadly used in detection of cerebral hemodynamics, there are always some contributions to the cortex signal from overlaying tissues (skin and skull), i.e., the partial volume effect (Durduran, 2004; Gagnon et al., 2012). More precise measurements of cerebral hemodynamics using multiple S–D separations and multi-layer theoretical models (Farrell et al., 1998) will be the subject of future work.

The sampling rate of ~2 Hz used in this study is sufficient for detecting LFO signals at ~0.1 Hz. However, measurements at this rate (2 Hz) may generate low frequency alias when sampling oscillations at the cardiac frequency (~1 Hz). Such low frequency alias may contaminate the LFO data. This contamination can be reduced by improving data acquisition rate as technology advances. For example, researchers have used spatially averaging method and few-mode detector fibers (instead of single-mode fibers) to achieve ~40 Hz sampling rate for DCS measurements while maintaining appropriate signal-to-noise ratios (Dietsche et al., 2007).

In the present study, we simply assume that LFOs of cerebral hemodynamics are only dependent of MAP oscillations. However, other variations may also affect the cerebral hemodynamics, notably partial pressures of end-tidal carbon dioxide (P_{ETCO₂}) and end-tidal oxygen (P_{ETO₂}) in particular during enforced breathing (Payne et al., 2009; Peng et al., 2008). Future study will concurrently monitor P_{ETCO₂} and P_{ETO₂} and use multi-input models to study cerebral hemodynamic LFOs.

Although the physiological manipulations used (i.e., HUT and enforced breathing) can significantly enhance LFOs, they may not be easily performed in some patient populations. For example, patients with vascular diseases may not be able to control their breathing at a low frequency of 0.1 Hz.

Conclusions

A novel hybrid NIR diffuse optical instrument was successfully used to simultaneously detect LFOs of CBF and cerebral oxygenation (i.e., [HbO₂], [Hb] and THC). Cerebral hemodynamic LFOs of both hemispheres were quantified and compared under three different physiological conditions (i.e., at rest, during HUT and during enforced breathing). We found that rCBF, Δ[HbO₂] and ΔTHC are reliable hemodynamic parameters in detecting LFOs and HUT is the most robust and stable protocol for quantifying phase shifts of LFOs in hemodynamic parameters. Comparing to other relevant studies, similar success rates in detecting cerebral LFOs were achieved in our study. Phase shifts of LFOs in CBF were close to those in CBFV reported by other groups, although the results in cerebral oxygenation measurements during enforced breathing varied across studies. Future study will investigate cerebral LFOs in patients with cerebral disease (e.g., carotid stenosis, stroke, neurocognitive impairment) and evaluate their cerebral autoregulation capabilities and neurocognitive functions via the quantification of LFO phase shifts. It is expected that direct and simultaneous measurements of LFOs in CBF and cerebral oxygenation will bring new and informative insights about mechanisms of cerebral autoregulation and pathologies of cerebral diseases.

Acknowledgments

We thank the support from the American Heart Association BGIA #2350015. We also thank Joyce M. Evens, Abhijit Patwardhan, David C. Randall, and Abner O. Rayapati for their beneficial discussions.

References

- Auer, D.P., 2008. Spontaneous low-frequency blood oxygenation level-dependent fluctuations and functional connectivity analysis of the 'resting' brain. *Magn. Reson. Imaging* 26, 1055–1064.
- Biswal, B., Yetkin, F.Z., Haughton, V.M., Hyde, J.S., 1995. Functional connectivity in the motor cortex of resting human brain using echo-planar MRI. *Magn. Reson. Med.* 34, 537–541.
- Biswal, B., VanKlyen, J., Hyde, J.S., 1997. Simultaneous assessment of flow and BOLD signals in resting-state functional connectivity maps. *NMR Biomed.* 10, 165–170.
- Boas, D.A., Yodh, A.G., 1997. Spatially varying dynamical properties of turbid media probed with diffusing temporal light correlation. *J. Opt. Soc. Am. A* 14, 192–215.
- Boas, D.A., Gaudette, T.J., Arridge, S.R., 2001. Simultaneous imaging and optode calibration with diffuse optical tomography. *Opt. Express* 8, 263–270.
- Bosomtvi, A., Jiang, Q., Ding, G.L., Zhang, L., Zhang, Z.G., Lu, M., Ewing, J.R., Chopp, M., 2008. Quantitative evaluation of microvascular density after stroke in rats using MRI. *J. Cereb. Blood Flow Metab.* 28, 1978–1987.
- Brown, W.R., Thore, C.R., 2011. Cerebral microvascular pathology in ageing and neurodegeneration. *Neuropathol. Appl. Neurobiol.* 37, 56–74.
- Cheung, C., Culver, J.P., Takahashi, K., Greenberg, J.H., Yodh, A.G., 2001. In vivo cerebrovascular measurement combining diffuse near-infrared absorption and correlation spectroscopies. *Phys. Med. Biol.* 46, 2053–2065.
- Cooper, R.J., Hebden, J.C., O'Reilly, H., Mitra, S., Michell, A.W., Everdell, N.L., Gibson, A.P., Austin, T., 2011. Transient haemodynamic events in neurologically compromised infants: a simultaneous EEG and diffuse optical imaging study. *Neuroimage* 55, 1610–1616.
- Culver, J.P., Siegel, A.M., Franceschini, M.A., Mandeville, J.B., Boas, D.A., 2005. Evidence that cerebral blood volume can provide brain activation maps with better spatial resolution than deoxygenated hemoglobin. *Neuroimage* 27, 947–959.
- Diehl, R.R., Linden, D., Lucke, D., Berlitz, P., 1995. Phase relationship between cerebral blood-flow velocity and blood-pressure – a clinical-test of autoregulation. *Stroke* 26, 1801–1804.
- Diehl, R.R., Linden, D., Lucke, D., Berlitz, P., 1998. Spontaneous blood pressure oscillations and cerebral autoregulation. *Clin. Auton. Res.* 8, 7–12.
- Diehl, R.R., Linden, D., Chalkiadaki, A., Diehl, A., 1999. Cerebrovascular mechanisms in neurocardiogenic syncope with and without postural tachycardia syndrome. *J. Auton. Nerv. Syst.* 76, 159–166.
- Dietsche, G., Ninck, M., Ortolfo, C., Li, J., Jaillon, F., Gisler, T., 2007. Fiber-based multispeckle detection for time-resolved diffusing-wave spectroscopy: characterization and application to blood flow detection in deep tissue. *Appl. Opt.* 46, 8506–8514.
- Duncan, A., Meek, J.H., Clemence, M., Elwell, C.E., Tyszczuk, L., Cope, M., Delpy, D.T., 1995. Optical pathlength measurements on adult head, calf and forearm and the head of the newborn infant using phase resolved optical spectroscopy. *Phys. Med. Biol.* 40, 295–304.
- Durduran, T., 2004. Non-Invasive Measurements of Tissue Hemodynamics with Hybrid Diffuse Optical Methods. Ph.D. thesis (University of Pennsylvania).

- Durduran, T., Yu, G., Burnett, M.G., Detre, J.A., Greenberg, J.H., Wang, J., Zhou, C., Yodh, A.G., 2004. Diffuse optical measurement of blood flow, blood oxygenation, and metabolism in a human brain during sensorimotor cortex activation. *Opt. Lett.* 29, 1766–1768.
- Durduran, T., Zhou, C., Edlow, B.L., Yu, G., Choe, R., Kim, M.N., Cucchiara, B.L., Putt, M.E., Shah, Q., Kasner, S.E., Greenberg, J.H., Yodh, A.G., Detre, J.A., 2009. Transcranial optical monitoring of cerebrovascular hemodynamics in acute stroke patients. *Opt. Express* 17, 3884–3902.
- Durduran, T., Zhou, C., Buckley, E.M., Kim, M.N., Yu, G., Choe, R., Gaynor, J.W., Spray, T.L., Durning, S.M., Mason, S.E., Montenegro, L.M., Nicolson, S.C., Zimmerman, R.A., Putt, M.E., Wang, J.J., Greenberg, J.H., Detre, J.A., Yodh, A.G., Licht, D.J., 2010. Optical measurement of cerebral hemodynamics and oxygen metabolism in neonates with congenital heart defects. *J. Biomed. Opt.* 15, 037004.
- Edlow, B.L., Kim, M.N., Durduran, T., Zhou, C., Putt, M.E., Yodh, A.G., Greenberg, J.H., Detre, J.A., 2010. The effects of healthy aging on cerebral hemodynamic responses to posture change. *Physiol. Meas.* 31, 477–495.
- Fantini, S., Franceschini, M.A., Gratton, E., 1994. Semi-infinite-geometry boundary-problem for light migration in highly scattering media – a frequency-domain study in the diffusion-approximation. *J. Opt. Soc. Am. B* 11, 2128–2138.
- Fantini, S., Hueber, D., Franceschini, M.A., Gratton, E., Rosenfeld, W., Stubblefield, P.G., Maulik, D., Stankovic, M.R., 1999. Non-invasive optical monitoring of the newborn piglet brain using continuous-wave and frequency-domain spectroscopy. *Phys. Med. Biol.* 44, 1543–1563.
- Farrell, T.J., Patterson, M.S., Essenpreis, M., 1998. Influence of layered tissue architecture on estimates of tissue optical properties obtained from spatially resolved diffuse reflectometry. *Appl. Opt.* 37, 1958–1972.
- Furlan, R., Porta, A., Costa, F., Tank, J., Baker, L., Schiavi, R., Robertson, D., Malliani, A., Mosqueda-Garcia, R., 2000. Oscillatory patterns in sympathetic neural discharge and cardiovascular variables during orthostatic stimulus. *Circulation* 101, 886–892.
- Gagnon, L., Desjardins, M., Jehanne-Lacasse, J., Bherer, L., Lesage, F., 2008. Investigation of diffuse correlation spectroscopy in multi-layered media including the human head. *Opt. Express* 16, 15514–15530.
- Gagnon, L., Yucel, M.A., Dehaes, M., Cooper, R.J., Perdue, K.L., Selb, J., Huppert, T.J., Hoge, R.D., Boas, D.A., 2012. Quantification of the cortical contribution to the NIRS signal over the motor cortex using concurrent NIRS-fMRI measurements. *Neuroimage* 59, 3933–3940.
- Haubrich, C., Wendt, A., Diehl, R.R., Klotzsch, C., 2004. Dynamic autoregulation testing in the posterior cerebral artery. *Stroke* 35, 848–852.
- Hu, H.H., Kuo, T.Y.B.J., Wong, W.J., Luk, Y.O., Chern, C.M., Hsu, L.C., Sheng, W.Y., 1999. Transfer function analysis of cerebral hemodynamics in patients with carotid stenosis. *J. Cereb. Blood Flow Metab.* 19, 460–465.
- Irwin, D., Dong, L., Shang, Y., Cheng, R., Kudrimoti, M., Stevens, S.D., Yu, G., 2011. Influences of tissue absorption and scattering on diffuse correlation spectroscopy blood flow measurements. *Biomed. Opt. Express* 2, 1969–1985.
- Julien, C., 2006. The enigma of Mayer waves: facts and models. *Cardiovasc. Res.* 70, 12–21.
- Katura, T., Tanaka, N., Obata, A., Sato, H., Maki, A., 2006. Quantitative evaluation of interrelations between spontaneous low-frequency oscillations in cerebral hemodynamics and systemic cardiovascular dynamics. *Neuroimage* 31, 1592–1600.
- Kim, M.N., Durduran, T., Frangos, S., Edlow, B.L., Buckley, E.M., Moss, H.E., Zhou, C., Yu, G., Choe, R., Maloney-Wilensky, E., Wolf, R.L., Grady, M.S., Greenberg, J.H., Levine, J.M., Yodh, A.G., Detre, J.A., Kofke, W.A., 2010. Noninvasive measurement of cerebral blood flow and blood oxygenation using near-infrared and diffuse correlation spectroscopies in critically brain-injured adults. *Neurocrit. Care* 12, 173–180.
- Levine, B.D., Giller, C.A., Lane, L.D., Buckley, J.C., Blomqvist, C.G., 1994. Cerebral versus systemic hemodynamic during graded orthostatic stress in humans. *Circulation* 90, 298–306.
- Li, J., Dietsche, G., Iftime, D., Skipetrov, S.E., Maret, G., Elbert, T., Rockstroh, B., Gsler, T., 2005. Noninvasive detection of functional brain activity with near-infrared diffusing-wave spectroscopy. *J. Biomed. Opt.* 10, 044002.
- Li, J., Ninck, M., Koban, L., Elbert, T., Kissler, J., Gsler, T., 2008. Transient functional blood flow change in the human brain measured noninvasively by diffusing-wave spectroscopy. *Opt. Lett.* 33, 2233–2235.
- Li, T., Gong, H., Luo, Q., 2011. Visualization of light propagation in visible Chinese human head for functional near-infrared spectroscopy. *J. Biomed. Opt.* 16, 045001.
- Marinoni, M., Ginanneschi, A., Forleo, P., Amaducci, L., 1997. Technical limits in transcranial Doppler recording: inadequate acoustic windows. *Ultrasound Med. Biol.* 23, 1275–1277.
- Mayer, S., 1876. Studien zur Physiologie des Herzens und der Blutgefäße. *Sitzungsberichte Akademie der Wissenschaften* 74, 281–307.
- Mcculloch, J., Edvinsson, L., Watt, P., 1982. Comparison of the effects of potassium and pH on the caliber of cerebral veins and arteries. *Pflug. Arch. Eur. J. Phys.* 393, 95–98.
- Morita, Y., Hardebo, J.E., Bouskela, E., 1995. Influence of cerebrovascular sympathetic, parasympathetic, and sensory nerves on autoregulation and spontaneous vasomotion. *Acta Physiol. Scand.* 154, 121–130.
- Munk, N., Symons, B., Shang, Y., Cheng, R., Yu, G., 2012. Noninvasively measuring the hemodynamic effects of massage on skeletal muscle: a novel hybrid near-infrared diffuse optical instrument. *J. Bodyw. Mov. Ther.* 16, 22–28.
- Nilsson, H., Aalkjaer, C., 2003. Vasomotion: mechanisms and physiological importance. *Mol. Interv.* 3, 79–89.51.
- Obrig, H., Neufang, M., Wenzel, R., Kohl, M., Steinbrink, J., Einhaupl, K., Villringer, A., 2000. Spontaneous low frequency oscillations of cerebral hemodynamics and metabolism in human adults. *Neuroimage* 12, 623–639.
- Panerai, R.B., 2008. Cerebral autoregulation: from models to clinical applications. *Cardiovasc. Eng.* 8, 42–59.
- Payne, S.J., Selb, J., Boas, D.A., 2009. Effects of autoregulation and CO₂ reactivity on cerebral oxygen transport. *Ann. Biomed. Eng.* 37, 2288–2298.
- Peng, T., Rowley, A.B., Ainslie, P.N., Poulin, M.J., Payne, S.J., 2008. Multivariate system identification for cerebral autoregulation. *Ann. Biomed. Eng.* 36, 308–320.
- Pogue, B.W., Paulsen, K.D., 1998. High-resolution near-infrared tomographic imaging simulations of the rat cranium by use of a priori magnetic resonance imaging structural information. *Opt. Lett.* 23, 1716–1718.
- Reinhard, M., Muller, T., Guschlbauer, B., Timmer, J., Hetzel, A., 2003. Transfer function analysis for clinical evaluation of dynamic cerebral autoregulation – a comparison between spontaneous and respiratory-induced oscillations. *Physiol. Meas.* 24, 27–43.
- Reinhard, M., Wehrle-Wieland, E., Grabiak, D., Roth, M., Guschlbauer, B., Timmer, J., Weiller, C., Hetzel, A., 2006. Oscillatory cerebral hemodynamics – the macro- vs. microvascular level. *J. Neurol. Sci.* 250, 103–109.
- Rice, S.O., 1954. *Mathematical analysis of random noise*. In: Wax, N. (Ed.), *Noise and Stochastic Processes*. Dover, New York, p. 133.
- Roche-Labarbe, N., Carp, S.A., Surova, A., Patel, M., Boas, D.A., Grant, P.E., Franceschini, M.A., 2010. Noninvasive optical measures of CBV, StO₂(2), CBF index, and rCMRO₂(2) in human premature neonates' brains in the first six weeks of life. *Hum. Brain Mapp.* 31, 341–352.
- Sassaroli, A., Zheng, F., Pierro, M., Bergethon, P.R., Fantini, S., 2011. Phase difference between low-frequency oscillations of cerebral deoxy- and oxy-hemoglobin concentrations during a mental task. *J. Innov. Opt. Health Sci.* 4, 151–158.
- Segal, S.S., 2005. Regulation of blood flow in the microcirculation. *Microcirculation* 12, 33–45.
- Shang, Y., Zhao, Y., Cheng, R., Dong, L., Irwin, D., Yu, G., 2009. Portable optical tissue flow oximeter based on diffuse correlation spectroscopy. *Opt. Lett.* 34, 3556–3558.
- Shang, Y., Chen, L., Toborek, M., Yu, G., 2011a. Diffuse optical monitoring of repeated cerebral ischemia in mice. *Opt. Express* 19, 20301–20315.
- Shang, Y., Cheng, R., Dong, L., Ryan, S.J., Saha, S.P., Yu, G., 2011b. Cerebral monitoring during carotid endarterectomy using near-infrared diffuse optical spectroscopies and electroencephalogram. *Phys. Med. Biol.* 56, 3015–3032.
- Tong, Y., Frederick, B.D., 2010. Time lag dependent multimodal processing of concurrent fMRI and near-infrared spectroscopy (NIRS) data suggests a global circulatory origin for low-frequency oscillation signals in human brain. *Neuroimage* 53, 553–564.
- van Beek, A.H., Claassen, J.A., Rikkert, M.G., Jansen, R.W., 2008. Cerebral autoregulation: an overview of current concepts and methodology with special focus on the elderly. *J. Cereb. Blood Flow Metab.* 28, 1071–1085.
- van Beek, A.H., Lagro, J., Olde-Rikkert, M.G., Zhang, R., Claassen, J.A., 2012. Oscillations in cerebral blood flow and cortical oxygenation in Alzheimer's disease. *Neurobiol. Aging* 33, 428.e21–31.
- Vern, B.A., Schuette, W.H., Leheta, B., Juel, V.C., Radulovacki, M., 1988. Low-frequency oscillations of cortical oxidative metabolism in waking and sleep. *J. Cereb. Blood Flow Metab.* 8, 215–226.
- Wang, K., Liang, M., Wang, L., Tian, L.X., Zhang, X.Q., Li, K.C., Jiang, T.Z., 2007. Altered functional connectivity in early Alzheimer's disease: a resting-state fMRI study. *Hum. Brain Mapp.* 28, 967–978.
- White, B.R., Snyder, A.Z., Cohen, A.L., Petersen, S.E., Raichle, M.E., Schlaggar, B.L., Culver, J.P., 2009. Resting-state functional connectivity in the human brain revealed with diffuse optical tomography. *Neuroimage* 47, 148–156.
- Yu, G., Durduran, T., Zhou, C., Wang, H.W., Putt, M.E., Saunders, H.M., Sehgal, C.M., Glatstein, E., Yodh, A.G., Busch, T.M., 2005. Noninvasive monitoring of murine tumor blood flow during and after photodynamic therapy provides early assessment of therapeutic efficacy. *Clin. Cancer Res.* 11, 3543–3552.
- Yu, G., Floyd, T., Durduran, T., Zhou, C., Wang, J.J., Detre, J.A., Yodh, A.G., 2007. Validation of diffuse correlation spectroscopy for muscle blood flow with concurrent arterial spin labeled perfusion MRI. *Opt. Express* 15, 1064–1075.
- Zhang, R., Zuckerman, J.H., Giller, C.A., Levine, B.D., 1998. Transfer function analysis of dynamic cerebral autoregulation in humans. *Am. J. Physiol. Heart Circ. Physiol.* 43, H233–H241.
- Zhou, C., Eucker, S., Durduran, T., Yu, G., Galston, J., Friess, S., Ichor, R., Margulies, S., Yodh, A.G., 2009. Diffuse optical monitoring of hemodynamic changes in piglet brain with closed head injury. *J. Biomed. Opt.* 14, 034015.
- Zirak, P., Delgado-Mederos, R., Marti-Fabregas, J., Durduran, T., 2010. Effects of acetazolamide on the micro- and macro-vascular cerebral hemodynamics: a diffuse optical and transcranial Doppler ultrasound study. *Biomed. Opt. Express* 1, 1443–1459.